Multi-Kernel Implicit Curve Evolution for Selected Texture Region Segmentation in VHR Satellite Images

Souleymane Balla-Arabé, *Member, IEEE*, Xinbo Gao, *Senior Member, IEEE*, Bin Wang, Fan Yang, and Vincent Brost

***Abstract*—Very high resolution (VHR) satellite images provide a mass of detailed information which can be used for urban planning, mapping, security issues, or environmental monitoring. Nevertheless, the processing of this kind of image is time-consuming, and extracting the needed information from among the huge quantity of data is a real challenge. For some applications such as natural disaster prevention and monitoring (typhoon, flood, bushfire, etc.), the use of fast and effective processing methods is demanded. Furthermore, such methods should be selective in order to extract only the information required to allow an efficient interpretation. For this purpose, we propose a texture region segmentation method using the level set algorithm and the multi-kernel theory. We design a selective and local multi-kernel stop function for which the regularization term depends on the fuzzy membership degree of a given pixel to be on the boundary or not. Favored by its local nature, the method is accelerated by means of an NVIDIA graphics processing unit programming. The new algorithm is selective, effective, and fast. Experimental results on VHR satellite images demonstrate subjectively and objectively the effectiveness of the proposed method.**

***Index Terms*—Fuzzy membership function, geometric active contours, graphics processing units (GPUs), image segmentation, partial differential equations.**

I. Introduction

In SOME remote sensing applications such as natural disaster prevention and monitoring, we need fast and effective processing methods since the information needs to be extracted and considered quickly. Furthermore, we are not interested in all of the huge quantity of information which can be provided by some high-resolution satellites like IKONOS, GeoEye-1, etc. For example, in the case of a volcano eruption or flooding monitoring, the most important task may be to know the contour of the active volcano or the flooded area. This task is more challenging because of the complexity and the textural richness of very high resolution (VHR) images. In this paper, our aim is to design a selective method which has the ability to give the user the choice of the texture he needs to segment. This characteristic is very important, for example, when monitoring a bush fire or flooded area. It should furthermore be a fast and effective image segmentation method for VHR satellite images. For remote sensing imagery, segmentation is used as an aid for landscape change detection or classification, road or building extraction [1]–[3], etc. The proposed method uses the level set method (LSM) and the multi-kernel technique in order to get a suitable segmentation result. The LSM [4]–[11] designates the class of active contour models (ACMs) which use the implicit representation of the evolving curve instead of the parametric one, i.e., the Lagrangian framework [12]. Fig. 1 displays the organization of ACMs. Our work was focused on LSM because of its intrinsic advantages, which allow easier handling of complex shapes and topological changes compared with parametric active contours, and its straightforward ability to pass from 2-D to 3-D. The LSM allows us also to easily add some constraint on the smoothness of the boundaries via some regularization terms. The basic idea of the LSM is to evolve the zero level of a given level set function (LSF) in the image domain until it reaches the boundaries of the regions of interest (ROIs). The active curve evolution is governed by the level set

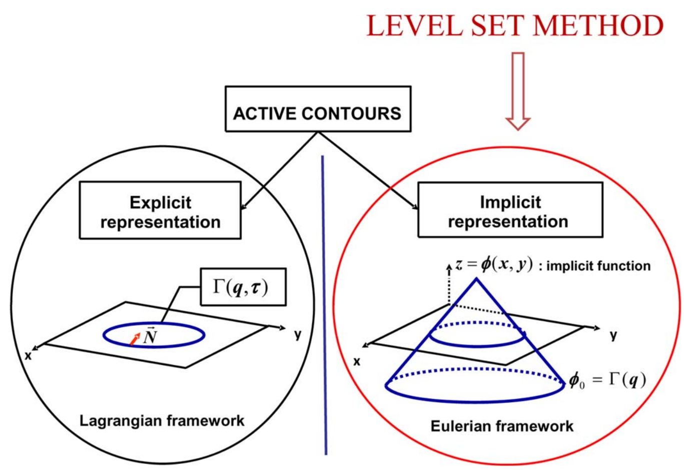

Fig. 1. Organization of ACMs.

Manuscript received January 16, 2013; revised May 11, 2013, June 10, 2013 and September 11, 2013; accepted October 17, 2013. Date of publication November 12, 2013; date of current version February 28, 2014. This work was supported in part by the National Natural Science Foundation of China under Grants 61125204, 61172146, and 41031064, by the Fundamental Research Funds for the Central Universities under Grant K5051202048, and by the Shaanxi Innovative Research Team for Key Science and Technology (No. 2012KCT-02).

S. Balla-Arabé, X. Gao, and B. Wang are with the State Key Laboratory of Integrated Services Networks, School of Electronic Engineering, Xidian University, Xi'an 710071, China (e-mail: balla_arabe_souleymane@ieee.org; xbgao@mail.xidian.edu.cn; bwang@xidian.edu.cn).

F. Yang and V. Brost are with the LE2I CNRS-UMR, Laboratory of Electronic, Computing and Imaging Sciences, University of Burgundy, 21078 Dijon, France (e-mail: fanyang@u-bourgogne.fr; vincent.brost@free.fr).

Color versions of one or more of the figures in this paper are available online at http://ieeexplore.ieee.org.

Digital Object Identifier 10.1109/TGRS.2013.2287239

equation (LSE). This is a partial differential equation and is defined as

$$\frac{\partial \phi}{\partial t} = V|\nabla \phi| \tag{1}$$

where ϕ is the LSF, $\nabla\phi$ is the gradient of ϕ, and V is the speed function which should drive and attract the evolution of the active contour toward the object boundaries. According to whether the speed function uses local or regional statistics, we can distinguish two general approaches, i.e., edge-based and region-based LSMs. The first one uses an edge indicator depending on the gradient of the image as in the classical snakes and ACMs [10]–[19], and these methods are effective when the boundaries of the object have a clear mutation in gray value. Nevertheless, they are more sensitive to noise and ineffective when the object of interest is without edges. The second approach uses some regional attributes to stop the evolving curve [20]–[23], and these methods are robust against noise, effective when detecting objects without edges, but have some difficulties when the boundaries between the object and the background are only defined by a high gradient.

Some works in the field of remote sensing imagery have already been done using the geometric active contour frameworks. Karantzalos *et al.* [39] developed a region-based level set algorithm for the automatic detection of man-made objects (roads, buildings, etc.) from aerial and satellite images. Bazi *et al.* [40] presented an unsupervised change detection method based on the piecewise constant Mumford–Shah model [41]. Nevertheless, these methods are not local and therefore not suitable for parallel programming using the graphics processing units (GPUs), for example. Their limitation is due to the fact that, at each iteration, the average intensities inside and outside the contour should be computed, which increases dramatically the executive time by increasing communications between processors.

In this paper, we first design a novel speed function based on the multi-kernel technique, which allows us to combine more information. Application of the multiple kernel technique has several advantages. In addition to the flexibility in selecting kernel functions, it also offers a possibility to combine different information from multiple heterogeneous or homogeneous sources. Typically, in an image segmentation context, the input data involved with the properties of the image pixels may be derived from totally different sources. For example, the intensity of a pixel is directly obtained from the image itself, while the texture information of a pixel might be obtained from some wavelet or Gabor filtering of the image. In our method, we combine kernels for intensity and texture information in order to obtain promising segmentation. Furthermore, the regularization term depends on the fuzzy membership degree of a given pixel to be on the boundary or not. We make the algorithm faster and suitable for GPU programming by using the lattice Boltzmann method (LBM) to solve the LSE. The local nature of the LBM, which makes it suitable for parallel programming, is not hindered since the designed speed function also has the advantage of using only local region statistics.

The LBM has only recently been used in image segmentation [24]–[26]. It is nevertheless very promising because of its simplicity and its intrinsic highly parallelizable nature. It has second-order accuracy both in time and space and can very well accelerate the LSM since the nonlinear term in the designed speed function, i.e., the regularization term, is implicitly computed. The LBM was originally designed to simulate Navier–Stokes equations for an incompressible fluid [27]–[29]. In our model, we use the D2Q5 ($D = 2$ and $b = 5$) LBM lattice structure. Fig. 2 displays a typical D2Q5 model. Each link has its velocity vector $e_i(\vec{r}, t)$ and the particle distribution $f_i(\vec{r}, t)$ that moves along this link, where $\vec{r}$ is the position of the cell and t is the time. The LBM evolution equation can be expressed as [30], [31]

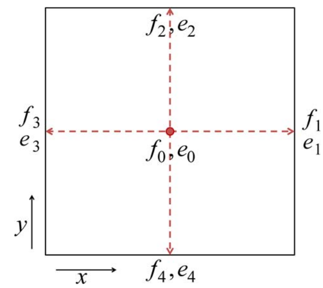

Fig. 2. Spatial structure of the D2Q5 LBM lattice.

$$f_i(\vec{r} + \vec{e}_i, t + 1) = f_i(\vec{r}, t) + \Omega_{\mathrm{BGK}} + \frac{D}{bc^2} \cdot \vec{F} \cdot \vec{e}_i \tag{2}$$

which can be decomposed into two steps

$$\text{Collision}: f^{\mathrm{coll}}(\vec{r},t) = f_i(\vec{r},t) + \Omega_{\mathrm{BGK}} + \frac{D}{bc^2} \cdot \vec{F}.\vec{e}_i \tag{3}$$

$$\text{Streaming}: f_i(\vec{r} + \vec{e}_i, t + 1) = f^{\mathrm{coll}}(\vec{r}, t) \tag{4}$$

where $\vec{F}$ is an external force, D is the grid dimension which is equal to 2 in this paper, b is the link at each grid point which is equal to 5 in this paper, c is the length of each link which is set to 1 in this paper, and Ω_{BGK} is the Bhatnager–Gross–Krook (BGK) collision model [26], [33] defined as

$$\Omega_{\mathrm{BGK}} = \frac{1}{\tau}\left[\bar{f}_i(\vec{r}, t) - f_i(\vec{r}, t)\right] \tag{5}$$

where τ represents the relaxation time and $\bar{f}_i$ is the local Maxwell–Boltzmann equilibrium particle distribution function expressed in its continuous form as

$$\bar{f}_i = \rho(2\pi RT)^{-3/2} \exp\left[-(\vec{v} - \vec{u})^2/2RT\right] \tag{6}$$

where $\vec{v}$ is the particle velocity, $\vec{u}$ is the macroscopic velocity, and ρ is the macroscopic fluid density. The equilibrium distribution can be expressed in discrete form as follows when modeling a typical diffusion phenomenon:

$$\bar{f}_i(\rho) = \rho A_i \qquad \text{with } \rho = \sum_i f_i. \tag{7}$$

By performing the Chapman–Enskog analysis [34], the following diffusion equation can be recovered from the LBM evolution equation [28]

$$\frac{\partial \rho}{\partial t} = \xi div(\nabla \rho) + F \tag{8}$$

where ξ is the diffusion coefficient and div is the divergence operator. Substituting ρ with the signed distance function ϕ in

(7), the LSE can be recovered. The body force F represents the image data link for the LBM solver.

Although some works for texture image segmentation using LSM have been done [5], [6], to our knowledge, there is no work presenting a selected texture segmentation method, i.e., the method which allows the user to choose the texture that he needs to segment. This intrinsic advantage allows the proposed methods to extract the object of interest from among a huge quantity of information provided by a VHR satellite image. Furthermore, the method is fast in enabling real-time applications. The regularization term used allows the method to be more accurate. Although any type of textural information can be used, experiments using a simple texture descriptor, incorporating the local mean value of the intensity and the standard variance, demonstrate the efficiency and the effectiveness of the proposed algorithm when segmenting textured images.

The remainder of this paper is organized as follows. Section II details the formulation of the proposed model. Experimental results are presented in Section III. Section IV concludes this paper.

II. Proposed Multi-Kernel LSM

This section describes the conception of the proposed local LSM. Let us consider the level set (1); in this paper, we propose the following multi-kernel speed function:

$$V(x)=\lambda\left(\varepsilon-(\theta_{\text{com}}(\psi(x))-\theta_{\text{com}}(I_t))^2\right)+V_{\text{reg}}(x) \tag{9}$$

where x is a spatial variable, I_t is the intensity of a given pixel belonging to the texture ROI, λ is a user-controlled positive parameter, and $\psi(x)=[I(x), I_f(x), s(x)] \in R^3$, in which $I(x) \in R$ is the intensity of pixel x. The two-tuple $[I_f(x), s(x)] \in R^2$ is a simple descriptor of the texture information at pixel x, where $I_f(x)$ is the filtered intensity of pixel x and $s(x)$ is the standard variance of the intensities of the pixels in the neighborhood of pixel x. ε is a positive and small constant, and θ_{com} is a transformation function defined through the following equation:

$$k_{\text{com}}(x,y)=\langle\theta_{\text{com}}(x)\theta_{\text{com}}(y)\rangle \tag{10}$$

where k_{com} is a nonnegative combination of two Mercer kernels k_1 and k_2:

$$k_{\text{com}}(x,y)=k_1(x,y)+\alpha * k_2(x,y) \qquad \text{with } \alpha>0. \tag{11}$$

In [38], the authors demonstrate that k_{com} is also a Mercer kernel. The commonly used kernels are linear, polynomial, and Gaussian kernels. Mathematical details about kernel creation can be seen in [38]. In this paper, we use the Gaussian kernel and define k_1 as a Gaussian kernel for pixel intensities and k_2 as a Gaussian kernel for texture information. They are formulated as follows:

$$k_1(x,y)=\exp\left[-\|I(x)-I(y)\|^2/\sigma^2\right] \tag{12}$$

$$k_2(x,y)=\exp\left[-\|[I_f(x),s(x)]-[I_f(y),s(y)]\|^2/\sigma^2\right] \tag{13}$$

where σ is the adjustable parameter.

A simple analysis of (9) shows that the proposed speed function tends to 0 when $(\theta_{\text{com}}(\psi(x))-\theta_{\text{com}}(I_t))^2$ tends to ε, which is a small value. Thus, the evolving contour will stop on a given pixel when its intensity and texture information are practically equal to those of the selected region. The main advantage of the designed speed function is that it is local and thus suitable for GPU-based acceleration.

Equation (9) can be rewritten as

$$\begin{aligned}V(x)&=\lambda\left(\varepsilon-(\theta_{\text{com}}(\psi(x))-\theta_{\text{com}}(I_t))^2\right)+V_{\text{reg}}(x)\\&=\lambda(\varepsilon-(\theta_{\text{com}}(\psi(x)).\theta_{\text{com}}(\psi(x))+\theta_{\text{com}}(I_t).\theta_{\text{com}}(I_t)\\&\quad-2\theta_{\text{com}}(\psi(x))\,\theta_{\text{com}}(I_t))+V_{\text{reg}}(x)\\&=\lambda(\varepsilon-(k_{\text{com}}(\psi(x),\psi(x))+k_{\text{com}}(\theta_{\text{com}}(I_t),\theta_{\text{com}}(I_t))\\&\quad-2\theta_{\text{com}}(\psi(x))\,\theta_{\text{com}}(I_t))+V_{\text{reg}}(x)\\&=\lambda\,(\varepsilon-2\,(1+\alpha-k_{\text{com}}(\psi(x),I_t)))+V_{\text{reg}}(x).\end{aligned} \tag{14}$$

From (10), (12), and (13), we have $k_{\text{com}}(\psi(x),I_t)=\theta_{\text{com}}(\psi(x))\theta_{\text{com}}(I_t)$, $k_{\text{com}}(\psi(x),\psi(x))=1+\alpha$, and $k_{\text{com}}(\theta_{\text{com}}(I_t), \theta_{\text{com}}(I_t))=1+\alpha$. Thus, (14) can be simplified as

$$V(x)=\lambda\,(\varepsilon-2\,(1+\alpha-k_{\text{com}}(\psi(x),I_t)))+V_{\text{reg}}(x). \tag{15}$$

The regularization term in (9) is defined as

$$V_{\text{reg}}(x)=\beta\,(1-\mu(x))+\nu div\,(\nabla\phi/|\nabla\phi|) \tag{16}$$

where x is a spatial variable, β and ν are positive constants, and μ is the fuzzy membership value of the pixel to be a boundary or not and is defined as

$$\begin{cases}\mu(x)=1-\frac{\eta-\delta}{\eta}, & \delta\le\eta\\ \mu(x)=1, & \delta>\eta\end{cases}$$

$$\text{where } \delta=|I(x)-I_{\text{mean}}(x)|,\ I_{\text{mean}}(x)=\frac{\int_\Omega s(x,y)I(y)dy}{\int_\Omega s(x,y)dy}$$

$$\text{and } s(x,y)=\begin{cases}1, & |x-y|<r\\ 0, & \text{otherwise.}\end{cases} \tag{17}$$

In the aforementioned equation, r is a radius constant, η a positive small parameter, and Ω is the image domain. Fig. 3 shows the μ-map of a given image. Thus, we can notice that, on the boundaries, the value of μ is close to unity (white pixels) and small for the background and object pixels (black pixels).

The first term of $V_{\text{reg}}(x)$ enforces the active contour to be as close as possible to those pixels for which $\mu(x)=1$, and the second term is the constraint on its length.

The proposed speed function can thus be rewritten as

$$\begin{aligned}V(x)=\lambda\,(\varepsilon-2\,(1+\alpha-k_{\text{com}}(\psi(x),I_t)))&\\+\beta\,(1-\mu(x))+\nu div\,(\nabla\phi/|\nabla\phi|)&\end{aligned} \tag{18}$$

and the proposed multi-kernel LSE is therefore

$$\begin{aligned}\frac{\partial\phi}{\partial t}=(\lambda\,(\varepsilon-2(1+\alpha-k_{\text{com}}(\psi(x),I_t)))&\\+\beta\,(1-\mu(x))+\nu div\,(\nabla\phi/|\nabla\phi|))\,|\nabla\phi|.&\end{aligned} \tag{19}$$

It is found that the designed speed function tends toward zero and stops the evolution of the active contour when $\theta_{\text{com}}(\psi(x))$

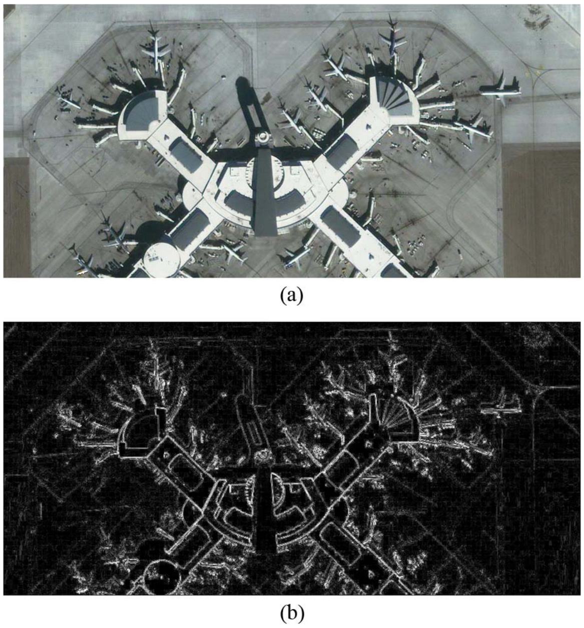

Fig. 3. Example of a μ-map on an IKONOS image of the McCarran International Airport, Las Vegas, NV, USA. (a) Original image. (b) Corresponding μ-map with $\eta = 0.2$.

is around the selected value $\theta_{\text{com}}(I_t)$, which represents the intensity and the texture information of the object of interest in the given scene.

To make the method suitable for parallel programming, we use the local LBM to solve the obtained LSE. Since we consider ϕ as a signed distance function, i.e., $|\nabla\phi| = 1$, (19) can therefore be expressed as

$$\frac{\partial\phi}{\partial t} = \lambda\left(\varepsilon - 2\left(1+\alpha - k_{\text{com}}\left(\psi(x), I_t\right)\right)\right) + \beta\left(1-\mu(x)\right) + \nu div(\nabla\phi) \quad (20)$$

which is similar to (8) with the body force expressed as

$$F = \lambda\left(\varepsilon - 2\left(1+\alpha - k_{\text{com}}\left(\psi(x), I_t\right)\right)\right) + \beta\left(1-\mu(x)\right). \quad (21)$$

The proposed LSE can therefore be solved using the following lattice Boltzmann evolution equation:

$$f_i(\vec{r}+\vec{e}_i, t+1) = f_i(\vec{r}, t) + \frac{1}{\tau}\left[\bar{f}_i(\vec{r}, t) - f_i(\vec{r}, t)\right] + \frac{D}{bc^2}\left(\lambda\left(\varepsilon - 2\left(1+\alpha - k_{\text{com}}\left(\psi(x), I_t\right)\right)\right) + \beta\left(1-\mu(x)\right)\right) \quad (22)$$

without the necessity of explicitly computing the curvature since it is implicitly handled by the LBM.

The principal implementation steps of the proposed method are as follows Fig. 4 illustrates the flowchart of the proposed multi-kernel level set algorithm, where we can clearly distinguish which part is executed on the CPU and which one on the GPU.

Input:	Initial zero level contour ϕ (signed distance function), ε, η, λ, α, β and σ.
Output:	The final zero level contour ϕ.
Algorithm Steps:	
1	Select a pixel in the region of interest (ROI), i.e., the textured region we want to segment.
2	Compute the membership matrix $\mu(x)$ with (17).
3	Compute the body force F with (21).
4	Resolve the LSE using LBM with (22).
5	Accumulate the $f_i(\vec{r}, t)$ values at each grid point with (7), which generates updated values of ϕ.
6	Find the contours.
7	If the segmentation is not done, increase the value of λ and go back to step 3.

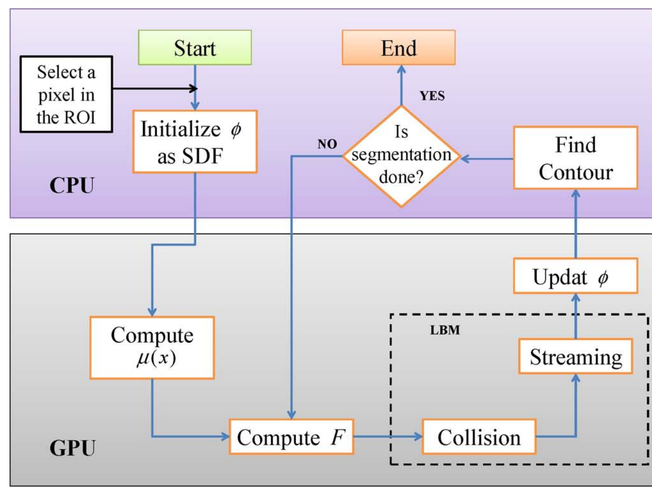

Fig. 4. Flowchart representing the process of the proposed algorithm.

III. Experimental Results and Analysis

In this section, we first describe the experimental framework. Second, a sensitivity analysis of the parameters used in the proposed method is done. Finally, we present the experimental results.

A. Experimental Setup

For the implementation of the proposed method, we used the parallel computing toolbox of MATLAB R2012a installed on a PC AMD Athlon 5200 processor with a clock speed of 2.31 GHz and 2 GB of RAM and possessing the NVIDIA GPU GT 430. We fixed $\varepsilon = 0.01$, $\eta = 0.2$, $\alpha = 2$, $\beta = 3.5$, $\sigma = 150$, and $\lambda = 100$. The optimized MATLAB function *arrayfun* is used to execute the code on the GPU.

The unsupervised objective evaluation is done by means of the Zeboudj's contrast [35] and the Rosenberger's criterion [36] as metrics. The first one takes into account the interior contrast of the regions in the neighborhood of each pixel, while the latter one takes into account the global intraclass and interclass disparities of each region of the image. The better the segmentation result is, the higher the two criteria are. For the supervised objective evaluation, we use the F-measure based on precision and recall, and the F-measure based on sensitivity and specificity (SF-measure). They measure the similarity between two images. The higher they are, the better the segmentation

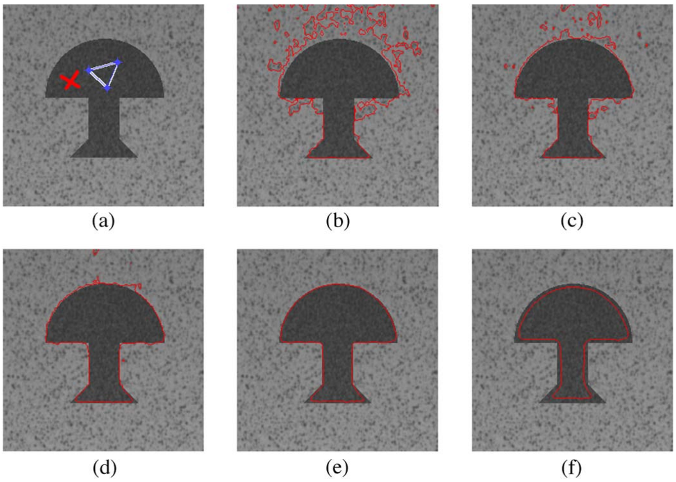

Fig. 5. Impact of the parameter α on the accuracy of the segmentation result. (a) Initial contour. (b) $\alpha = 0.5$, and $\beta = 3.5$. (c) $\alpha = 0.75$, and $\beta = 3.5$. (d) $\alpha = 1$, and $\beta = 3.5$. (e) $\alpha = 2$, and $\beta = 3.5$. (f) $\alpha = 10$, and $\beta = 3.5$.

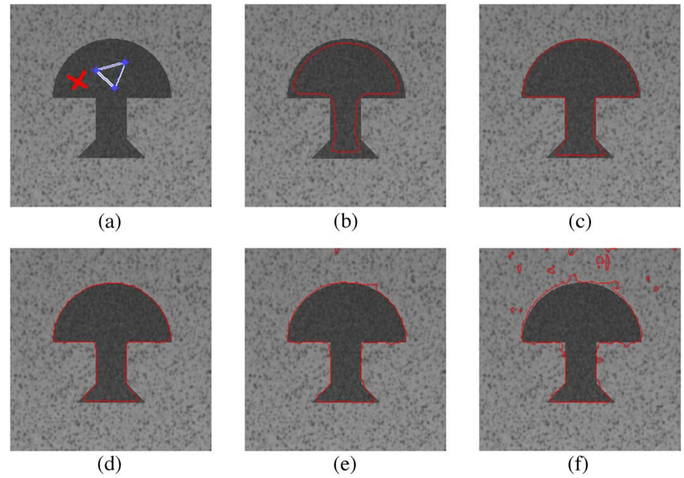

Fig. 6. Impact of the parameter β on the accuracy of the segmentation result. (a) Initial contour. (b) $\alpha = 2$, and $\beta = 1$. (c) $\alpha = 2$, and $\beta = 2.5$. (d) $\alpha = 2$, and $\beta = 3.5$. (e) $\alpha = 2$, and $\beta = 4$. (f) $\alpha = 2$, and $\beta = 5$.

result is. As suggested in [42] and [43], each ground truth used for the supervised evaluation is the average of three experts' manual segmentation.

In all of the experimental results, the interior of the final LSF is represented by black pixels, and the exterior is represented by white pixels. The blue triangle is the initial contour, and the red cross indicates the texture of interest. The dimensions of the images used are 450×948.

The proposed method and all of the methods used for comparison were run using the intensity information I of multispectral images, which is obtained by performing a weighted sum of the R, G, and B components as recommended by the 601 resolution of the International Commission on Illumination (CIE)

$$I = 0.2989 \times R + 0.5870 \times G + 0.1140 \times B. \tag{23}$$

B. Sensitivity Analysis

In the case of 2-D image segmentation, a 2-D lattice structure should be used in the LBM solver. We use here the D2Q5 model, i.e., $D = 2$, and $b = 5$. Thus, $D/bc^2 = 0.4$ when the length of each link c is set to 1. The parameter λ can be used to accelerate the convergence of the proposed method toward the steady state, τ is used to implicitly control the curvature, and α controls the impact of the texture information on the segmentation result. In order to well segment the textured ROI, a suitable value of α should be selected. A too high value can lead to undersegmentation, while a too low value will definitively lead to an oversegmented result. Figs. 5 and 6 show the impact of the parameters α and β on the segmentation result. The blue triangle is the initial contour, and the red cross indicates the texture of interest. We can effectively see that a too low value of $\alpha (\alpha = 0.5)$ leads to an oversegmentation, while a too high value $(\alpha = 10)$ decreases the precision of the result (undersegmentation). We can also see that a too low value of β leads to an undersegmented result as the curve fails to detect the right contour. That is why in all of the experimental section we fixed $\alpha = 2$ and $\beta = 3.5$.

C. Experimental Result

Fig. 7 demonstrates the ability of the proposed image segmentation method in terms of selectivity. The original image was taken by IKONOS in May 2011 and shows the General DeWitt Spain Airport after flooding. The red cross indicates the texture that we want to segment and thus determines the value of I_t, and the blue triangle indicates the initial contour of the C-V and the proposed method. In the first row, where we wanted to segment the white houses, we can see that the experimental result is more than promising. In the second row, where we wanted to extract just the flooded area, we can also see the quality of the segmentation result. In the third row, we want to segment the trees at the right-hand side of the picture, which have a particular texture, and the segmentation result is also adequate.

From Figs. 8–12, we can compare the performance of the proposed method, in terms of selectivity, with five well known segmentation methods running on a CPU: the C-V method [23], the fuzzy c-means (FCM), the K-means, the recent parametric kernel graph cuts (PKGC) based image segmentation method introduced in [37], and the one class support vector machine (SVM) using a Gaussian radial basis function kernel with a scaling factor of one. The executive times and the results of the unsupervised objective evaluation are displayed in Tables I–V.

Fig. 8 shows the McCarran International Airport of Las Vegas taken by IKONOS in January 2011. In this experiment, our purpose is to segment the white objects. We can see that the C-V method gets trapped into a local minimum and just extracts a part of the area. The FCM, the K-means, and the one class SVM give an oversegmented result by including many unwanted regions in the desired cluster. The proposed method extracts the white objects better and is faster even than K-means, which is nevertheless deemed to be fast. The PKGC gives a good result, but the proposed method outperforms it in terms of executive time and Zeboudj's and Rosenberger's measures.

Fig. 9 was taken by GeoEye-1. We notice again that the proposed method has extracted the limit of water better than the other methods and again has the highest Zeboudj's and

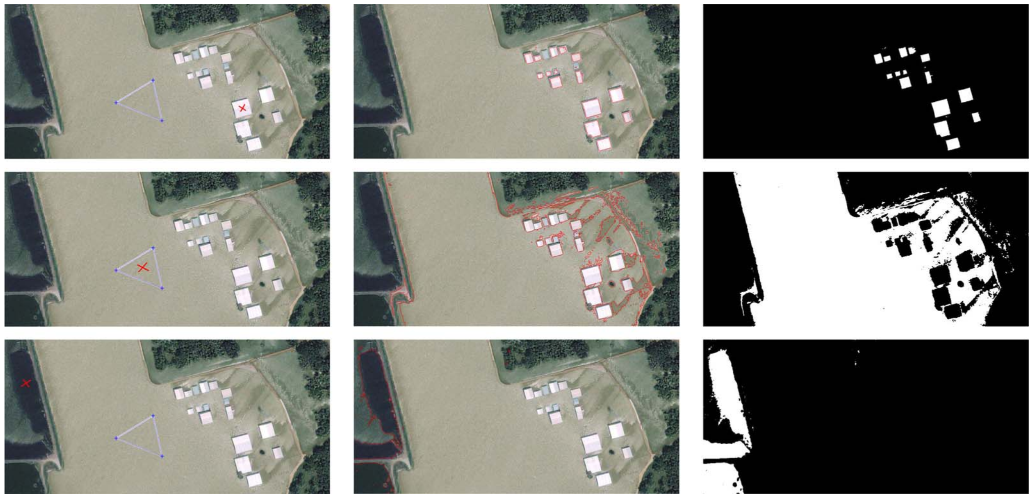

Fig. 7. IKONOS image of the General DeWitt Spain Airport after flooding. In the first column, we have the original image in which the red cross selects the texture that we want to segment and the blue triangle is the initial contour of the proposed LSM. The segmentation results are displayed in the second and third columns. The second column shows the final LSF. In the third column, the interior of the final LSF is represented by black pixels and the exterior by white pixels.

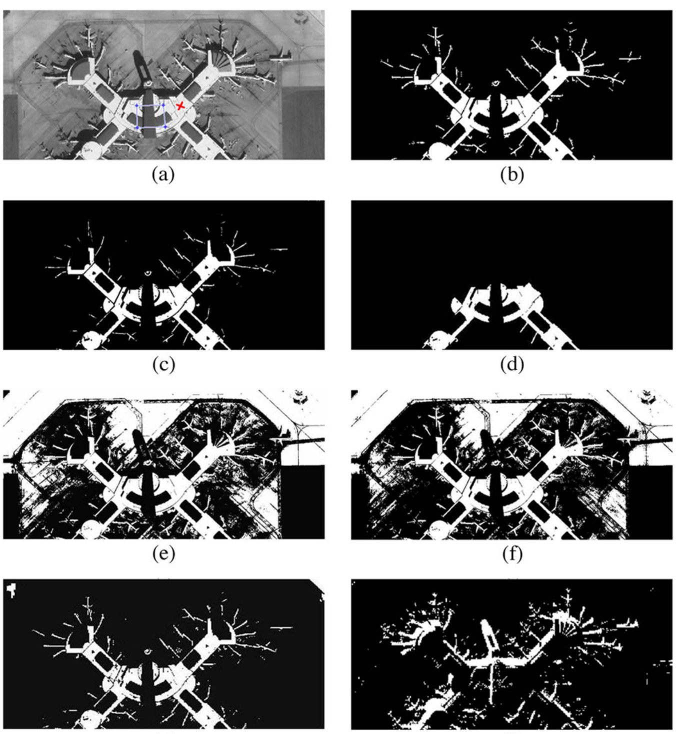

(a) (b) (c) (d) (e) (f) (g) (h)

Fig. 8. IKONOS image of the McCarran International Airport of Las Vegas. (a) Original image. (b) Ground truth image. (c) Segmentation result of the proposed method. (d) Segmentation result of the C-V method. (e) Segmentation result of the FCM algorithm. (f) Segmentation result of the K-means algorithm. (g) Segmentation result of the PKGC algorithm. (h) Segmentation result using one class SVM.

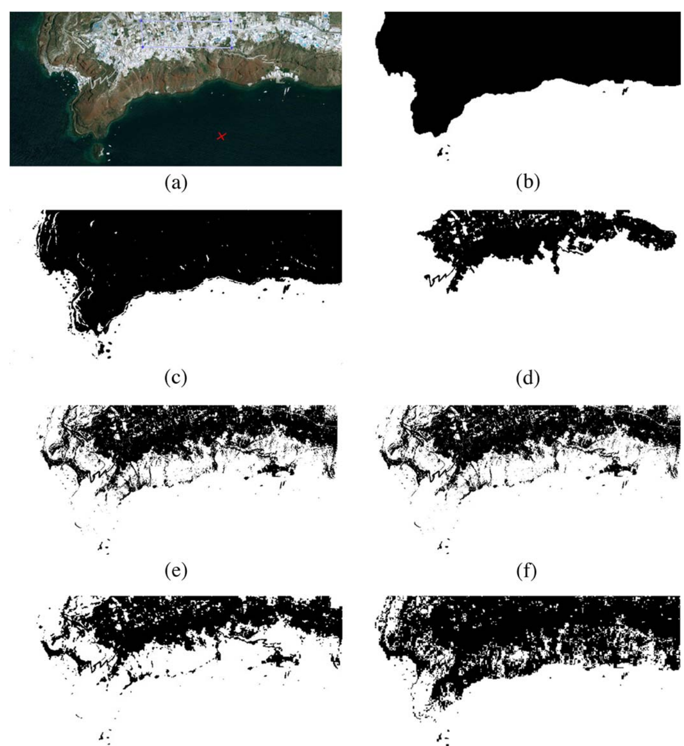

(a) (b) (c) (d) (e) (f) (g) (h)

Fig. 9. Image taken by GeoEye-1. (a) Original image. (b) Ground truth image. (c) Segmentation result of the proposed method. (d) Segmentation result of the C-V method. (e) Segmentation result of the FCM algorithm. (f) Segmentation result of the K-means algorithm. (g) Segmentation result of the PKGC algorithm. (h) Segmentation result using one class SVM.

Rosenberger's measures. That means that it can be effective when used for flooding prevention or monitoring.

Fig. 10 was taken by IKONOS. We notice that most of the methods have delimitated the active volcano well. However, the proposed method, the C-V method, and the PKGC method have delimitated the forest area better.

Figs. 11 and 12 are also IKONOS images. Fig. 11 is the image of Uxmal in Mexico taken in 2002. It demonstrates the ability of the proposed method in terms of damaged or nonforested areas and road extraction in a forest area. The C-V method gets trapped into a local minimum and gives an undersegmented result. The FCM and the one class SVM give an oversegmented result. The proposed method and the PKGC give the best results by extracting the real roads and nonforest areas very well. It can be seen that the proposed method is again the fastest one and has the highest Zeboudj's and Rosenberger's measures. That means that it can be efficient when used for agriculture monitoring or detection of damaged regions after

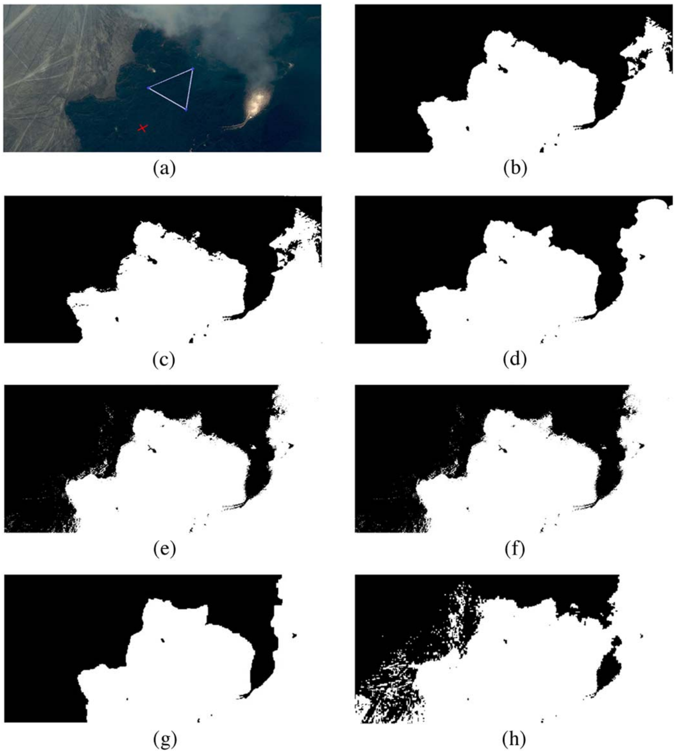

Fig. 10. Image taken by IKONOS. (a) Original image. (b) Ground truth image. (c) Segmentation result of the proposed method. (d) Segmentation result of the C-V method. (e) Segmentation result of the FCM algorithm. (f) Segmentation result of the K-means algorithm. (g) Segmentation result of the PKGC algorithm. (h) Segmentation result using one class SVM.

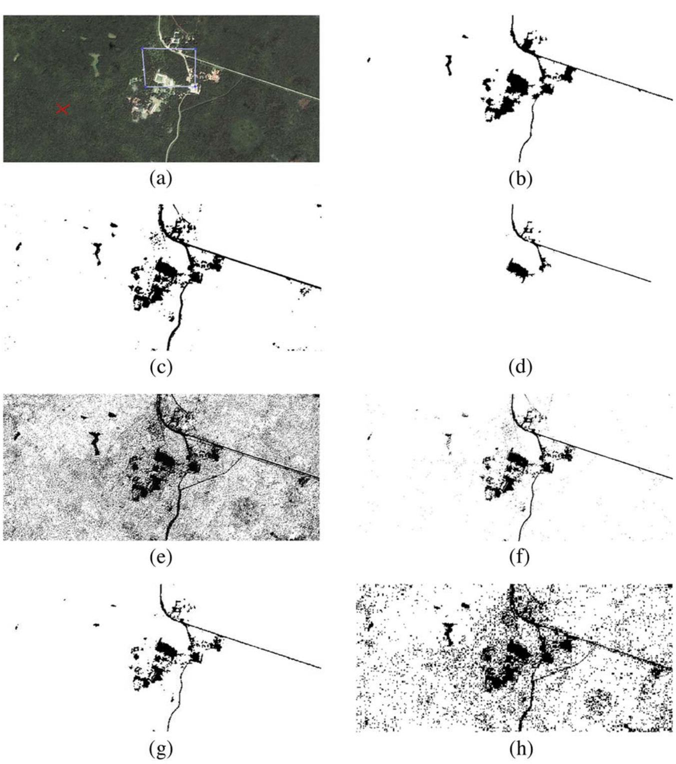

Fig. 11. IKONOS image of Uxmal in Mexico. (a) Original image. (b) Ground truth image. (c) Segmentation result of the proposed method. (d) Segmentation result of the C-V method. (e) Segmentation result of the FCM algorithm. (f) Segmentation result of the K-means algorithm. (g) Segmentation result of the PKGC algorithm. (h) Segmentation result using one class SVM.

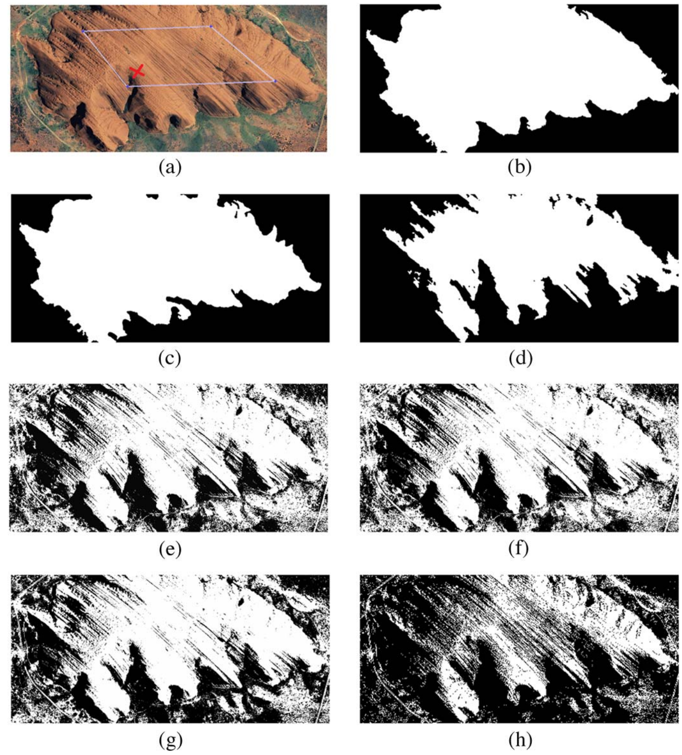

Fig. 12. IKONOS image of Ayers rock in Australia. (a) Original image. (b) Ground truth image. (c) Segmentation result of the proposed method. (d) Segmentation result of the C-V method. (e) Segmentation result of the FCM algorithm. (f) Segmentation result of the K-means algorithm. (g) Segmentation result of the PKGC algorithm. (h) Segmentation result using one class SVM.

natural disasters such as wildfires. Fig. 12 represents the Ayers rock in Australia. We can subjectively see that the method that we introduced in this paper extracts the rock better. The objective evaluation confirms this promising result.

Table VI displays the statistical results of the supervised objective evaluation of the proposed algorithm using the F-measure and the SF-measure. It can be seen that, in all of the cases, the proposed method has the highest measure of similarity. It therefore gives better segmentation results.

It can also be seen that the proposed method is fast. When comparing the CPU time, it can be seen that only the well-known fast K-means is faster than the proposed method. The GPU implementation shows the suitability of the proposed method for parallel programming. Furthermore, the GPU implementation would be far faster if done using CUDA C instead of MATLAB.

Nevertheless, we should note that the proposed method is highly dependent on the initial selected pixel which determines the region to be segmented. This can be a limitation when used in automatic systems.

IV. Conclusion and Perspectives

In this paper, we have presented a segmentation method for VHR satellite images. The method combines the advantage of the LSM and the multi-kernel technique. This allows it to easily handle complex shapes and to simultaneously incorporate intensity and texture information in the segmentation process. The method is efficient and effective when segmenting textured VHR images. The selectivity of the method allows extraction of

TABLE I
COMPARISON OF EXECUTIVE TIMES AND OBJECTIVE EVALUATIONS USING IKONOS IMAGE OF THE MCCARRAN INTERNATIONAL AIRPORT OF LAS VEGAS

Methods	**C-V**	**FCM**	**K-means**	**PKGC**	**One class SVM**	**Our method**
Executive time(s)	225.123	33.862	1.687	3.4300	503.27	CPU 2.907 GPU 0.814
Zeboudj criterion	0.47	0.34	0.37	0.49	0.48	0.57
Rosenberger criterion	0.70	0.46	0.50	0.73	0.59	0.90
F-measure (%)	89.935	79.891	81.031	86.232	85.105	98.553
SF-measure (%)	78.724	58.748	59.314	63.647	62.743	90.331

TABLE II
COMPARISON OF EXECUTIVE TIMES AND OBJECTIVE EVALUATIONS USING AN IMAGE TAKEN BY GeoEye-1

Methods	**C-V**	**FCM**	**K-means**	**PKGC**	**One class SVM**	**Our method**
Executive time(s)	187.97	41.176	1.526	3.4626	651.994	CPU 2.945 GPU 0.736
Zeboudj criterion	0.48	0.52	0.51	0.47	0.57	0.58
Rosenberger criterion	0.73	0.70	0.75	0.74	0.82	0.86
F-measure (%)	86.002	80.403	82.775	85.047	88.507	97.080
SF-measure (%)	77.228	59.721	59.887	62.312	81.332	87.047

TABLE III
COMPARISON OF EXECUTIVE TIMES AND OBJECTIVE EVALUATIONS USING AN IKONOS IMAGE OF A VOLCANO

Methods	**C-V**	**FCM**	**K-means**	**PKGC**	**One class SVM**	**Our method**
Executive time(s)	371.15	26.068	1.088	2.8583	509.786	CPU 2.739 GPU 0.759
Zeboudj criterion	0.54	0.51	0.52	0.53	0.49	0.57
Rosenberger criterion	0.87	0.73	0.74	0.82	0.71	0.88
F-measure (%)	92.586	81.225	79.422	85.412	81.977	97.123
SF-measure (%)	77.347	62.843	62.449	63.420	61.455	88.786

TABLE IV
COMPARISON OF EXECUTIVE TIMES AND OBJECTIVE EVALUATIONS USING AN IKONOS IMAGE OF UXMAL IN MEXICO

Methods	**C-V**	**FCM**	**K-means**	**PKGC**	**One class SVM**	**Our method**
Executive time(s)	569.716	39.525	3.512	5.3106	890.579	CPU 3.401 GPU 0.898
Zeboudj criterion	0.47	0.41	0.51	0.50	0.45	0.54
Rosenberger criterion	0.73	0.50	0.77	0.74	0.70	0.89
F-measure (%)	90.013	79.973	82.896	84.377	80.304	97.848
SF-measure (%)	78.013	59.623	61.180	61.993	60.993	90.044

only the information of interest from among the vast quantity of information contained in a VHR image. This is of great importance for an optimal interpretation of the segmentation result.

In order to make the proposed method faster and therefore more suitable for real-time volume image segmentation, future work will be on the implementation of the body force and the streaming step of LBM using a field-programmable gate array (FPGA). This choice is influenced by the fact that these two steps need neighborhood pixels to be performed, and in this case, the FPGA could be more efficient than the GPU because of its flexible memory system.

TABLE V
COMPARISON OF EXECUTIVE TIMES AND OBJECTIVE EVALUATIONS USING AN IKONOS IMAGE OF AYERS ROCK

Methods	**C-V**	**FCM**	**K-means**	**PKGC**	**One class SVM**	**Our method**
Executive time(s)	238.07	11.65	1.892	3.116	603.790	CPU 3.002 GPU 0.591
Zeboudj criterion	0.49	0.43	0.42	0.45	0.40	0.52
Rosenberger criterion	0.67	0.65	0.64	0.72	0.63	0.79
F-measure (%)	88.117	81.901	81.928	84.779	80.032	96.738
SF-measure (%)	77.903	58.764	58.530	62.728	60.099	88.339

TABLE VI
STATISTICAL RESULTS OF THE OBJECTIVE EVALUATION USING F-MEASURE AND SF-MEASURE

	F-measure (%)	**SF-measure (%)**	**F-measure (%)**	**SF-measure (%)**
	Average		**Standard deviation**	
Our method	97.4684	88.9094	0.7287	1.3339
C-V	89.3306	77.8430	2.4485	0.5985
FCM	80.6786	59.9398	0.8641	1.6867
K-means	81.6104	60.2720	1.4348	1.5544
PKGC	85.1694	62.8200	0.7041	0.7061
One class SVM	83.1850	65.3244	3.5955	8.9992

REFERENCES

[1] B. Yang, Z. Wei, Q. Li, and J. Li, "Semiautomated building façade footprint extraction from mobile LiDAR point clouds," *IEEE Geosci. Remote Sens. Letters*, vol. 10, no. 4, pp. 766–770, Jul. 2013.

[2] Y. Bazi, F. Melgani, and H. Al-Sharari, "Use of salient feature for the design of a multistage framework to extract roads from high-resolution multispectral satellite," *IEEE Trans. Geosci. Remote Sens.*, vol. 49, no. 10, pp. 3906–3931, Oct. 2011.

[3] P. Gamba and M. Aldrighi, "SAR data classification of urban areas by means of segmentation techniques and ancillary optical data," *IEEE J. Select. Top. Appl. Earth Observ. Remote Sens.*, vol. 5, no. 4, pp. 1140–1148, Sep. 2012.

[4] J. Ball and L. Bruce, "Level set hyperspectral image classification using best band analysis," *IEEE Trans. Geosci. Remote Sens.*, vol. 45, no. 10, pp. 3022–3027, Oct. 2007.

[5] J.-F. Aujol, G. Aubert, and L. Blanc-Féraud, "Wavelet-based level set evolution for classification of textured images," *IEEE. Trans. Image Process.*, vol. 12, no. 12, pp. 1634–1641, Dec. 2003.

[6] I. Karaoui, R. Fablet, J.-M. Boucher, and J.-M. Augustin, "Region-based image segmentation using texture statistics and level set methods," in *Proc. IEEE Int. Conf. Acoustics, Speech and Signal Processing*, Toulouse, 2006, vol. 2, p. II.

[7] S. Balla-Arabé and X.-B. Gao, "Image multi-thresholding by combining the lattice Boltzmann model and a localized level set algorithm," *Neurocomputing*, vol. 93, pp. 106–114, 2012.

[8] H. Hichri, Y. Bazi, N. Alajlan, and S. Malek, "Interactive segmentation for change detection in multispectral remote-sensing image," *IEEE Geosci. Remote Sens. Letters*, vol. 10, no. 2, pp. 298–302, Mar. 2013.

[9] G. Akbarizadeh, "A new statistical-based kurtosis wavelet energy feature for texture recognition of SAR images," *IEEE Trans. Geosci. Remote Sens.*, vol. 50, no. 11, pp. 4358–4368, Nov. 2012.

[10] K. Karantzalos and N. Paragios, "Recognition-driven two-dimensional competing priors toward automatic and accurate building detection," *IEEE Trans. Geosci. Remote Sens.*, vol. 47, no. 1, pp. 133–144, Jan. 2009.

[11] Y. Huang and Y. Huang, "Segmenting SAR satellite images with the multilayer level set approach," *IEEE J. Select. Top. Appl. Earth Observ. Remote Sens.*, vol. 4, no. 3, pp. 632–642, Sep. 2011.

[12] S. Zhu and A. Yuille, "Region competition: Unifying snakes, region growing, and Bayes/MDL for multiband image segmentation," *IEEE Trans. Pattern Anal. Mach. Intell.*, vol. 18, no. 9, pp. 884–900, Sep. 1996.

[13] C. Brun, N. Leporé, X. Pennec, Y. Chou, A. Lee *et al.*, "A nonconservative Lagrangian framework for statistical fluid registration–SAFIRA," *IEEE Trans. Med. Imag.*, vol. 30, no. 2, pp. 184–202, 2011.

[14] X.-B. Gao, B. Wang, D. Tao, and X. Li, "A relay level set method for automatic image segmentation," *IEEE Trans. Syst., Man, Cybern., Part B: Cybern.*, vol. 41, no. 2, pp. 518–525, Apr. 2011.

[15] M. Kass, A. Witkin, and D. Terzopoulos, "Snakes: Active contour models," *Int. J. Comp. Vis.*, vol. 1, no. 4, pp. 321–331, 1988.

[16] V. Casselles, F. Catté, and F. Dibos, "A geometric model for active contours in image processing," *Numerische Mathematik*, vol. 66, pp. 1–31, 1993.

[17] L. D. Cohen, "On active contour models and balloons," *Comput. Vis., Graph., Image Process.*, vol. 53, no. 2, pp. 211–218, 1991.

[18] R. Malladi, J. Sethian, and B. Vemuri, "A topology independent shape modeling scheme," in *Proc. SPIE Conf. Geometric Methods in Computer Vision II*, San Diego, CA, 1993, vol. 2031, pp. 246–258.

[19] V. Caselles, R. Kimmel, and G. Sapiro, "On geodesic active contours," *Int. J. Comput. Vis.*, vol. 22, no. 1, pp. 61–79, 1997.

[20] N. Paragios and R. Deriche, "Geodesic active contours for supervised texture segmentation," in *Proc. IEEE Conf. Computer Vision and Pattern Recognition (CVPR)*, 1999, pp. I: 1034–I: 1040.

[21] M. Silveira and S. Heleno, "Separation between water and land in SAR images using region-based level sets," *IEEE Geosci. Remote Sens. Letters*, vol. 6, no. 3, pp. 471–475, Jul. 2009.

[22] S. Balla-Arabé, B. Wang, and X.-B. Gao, "Level set region based image segmentation using lattice Boltzmann method," in *Proc. 7th Int. Conf. Computational Intelligence and Security*, Sanya, China, Dec. 2011, pp. 1159–1163.

[23] T. Chan and L. Vese, "Active contours without edges," *IEEE. Trans. Image Process.*, vol. 10, no. 2, pp. 266–277, 2001.

[24] Y. Chen, Z. Yan, and Y. Chu, "Cellular automata based level set method for image segmentation," in *Proc. IEEE/ICME Int. Conf. Complex Medical Engineering*, Beijing, China, May 2007, pp. 23–27.

[25] S. Balla-Arabé, X.-B. Gao, and B. Wang, "A fast and robust level set method for image segmentation using fuzzy clustering and lattice Boltzmann method," *IEEE Trans. Syst., Man, Cybern., Part B: Cybern.*, vol. 43, no. 3, pp. 910–920, 2013.

[26] S. Balla-Arabé, X.-B. Gao, and B. Wang, "GPU accelerated edge-region based level set evolution constrained by 2D gray-scale histogram," *IEEE. Trans. Image Process.*, vol. 22, no. 7, pp. 2688–2698, Jul. 2013.

[27] S. Succi, *The Lattice Boltzmann Equation for Fluid Dynamics and Beyond Numerical Mathematics and Scientific Computation*. New York: Oxford Univ. Press, 2001.

[28] Y. Zhao, "Lattice Boltzmann based PDE solver on the GPU," *Visual Comput.*, vol. 24, no. 5, pp. 323–333, May 2007, Springer.

[29] X. He and L. Luo, "Lattice Boltzmann model for incompressible Navier–Stokes equation," *J. Stat. Phys.*, vol. 88, no. 3–4, pp. 927–944, 1997.

[30] X. Shan and G. Doolen, *J. Stat. Phys.*, vol. 81, p. 379, 1995.

[31] I. Ginzbourg and P. M. Adler, *J. Phys. II*, vol. 4, p. 191, 1994.

[32] P. L. Bhatnager, E. P. Gross, and M. Krook, *Phys. Rev.*, vol. 94, p. 511, 1954.

[33] J. Buick and C. Greated, “Gravity in a lattice Boltzmann model,” *Phys. Rev. E*, vol. 61, no. 5, pp. 5307–5320, 2000.

[34] S. Chapmann and T. G. Cowling, *The Mathematical Theory of Non-Uniform Gases: An Account of the Kinetic Theory of Viscosity, Thermal Conduction and Diffusion in Gases*. Cambridge, U.K.: Cambridge Univ. Press, 1990.

[35] R. Zeboudj, “Filtrage, seuillage automatique, contraste et contours: Du pré-traitement à l’analyse d’images,” PhD thesis, Saint Etienne University, 1988.

[36] C. Rosenberger and K. Chehdi, “Genetic fusion: Application to multi-components image segmentation,” in *Proc. IEEE Int. Conf. Acoustics, Speech and Signal Processing*, Istanbul, Turkey, 2000, pp. 2219–2222.

[37] M. Ben Salah, A. Mitiche, and I. Ben Ayed, “Multiregion image segmentation by parametric kernel graph cuts,” *IEEE. Trans. Image Process.*, vol. 20, no. 2, pp. 545–557, Feb. 2011.

[38] N. Christianini and J. Shawe-Taylor, *An Introduction to Support Vector Machines*. Cambridge, UK: Cambridge Univ. Press, 2000.

[39] K. Karantzalos and D. Argiala, “A region-based level set segmentation for automatic detection of man-made objects from aerial and satellite images,” *Photogramm. Eng. Remote Sens.*, vol. 75, no. 6, pp. 667–677, 2009.

[40] Y. Bazi, F. Melgani, and H. Al-Sharari, “Level set hyperspectral image classification using best band analysis,” *IEEE Trans. Geosci. Remote Sens.*, vol. 48, no. 8, pp. 3178–3187, Aug. 2010.

[41] D. Mumford and J. Shah, “Optimal approximations by piecewise smooth functions and associated variational problems,” *Commun. Pure Appl. Math.*, vol. 42, no. 5, pp. 577–685, 1989.

[42] N. Situ, X. Yuan, G. Zouridakis, and N. Mullani, “Automatic segmentation of skin lesion images using evolutionary strategy,” in *Proc. IEEE Int. Conf. Image Processing (ICIP)*, 2007, vol. 6, pp. 277–280.

[43] X. Yuan, N. Situ, and G. Zouridakis, “A narrow band graph partitioning method for skin lesion segmentation,” *Pattern Recog.*, vol. 42, no. 6, pp. 1017–1028, 2009.

Souleymane Balla-Arabé (M’12) received the M.Eng. degree in electronic from Polytechnic Military School, Algiers, Algeria, in 2004. He is currently working toward the Ph.D. degree in information and communication engineering in the State Key Laboratory of Integrated Services Networks, Xidian University, Xi’an, China.

In May 2013, he was an Invited Researcher at LE2I CNRS-UMR, Laboratory of Electronic, Computing and Image Sciences, University of Burgundy, Dijon, France. His current research interests include variational methods for image segmentation, computational intelligence, and machine learning.

Xinbo Gao (M’02–SM’07) received the B.Eng., M.Sc., and Ph.D. degrees in signal and information processing from Xidian University, Xi’an, China, in 1994, 1997, and 1999, respectively.

From 1997 to 1998, he was a Research Fellow with the Department of Computer Science, Shizuoka University, Shizuoka, Japan. From 2000 to 2001, he was a Postdoctoral Research Fellow with the Department of Information Engineering, Chinese University of Hong Kong, Shatin, Hong Kong. Since 2001, he has been with the School of Electronic Engineering, Xidian University, where he is currently a Professor of pattern recognition and intelligent system and the Director of the VIPS Laboratory. He is on the editorial boards of several journals including *Signal Processing* (Elsevier) and *Neurocomputing* (Elsevier). His research interests are computational intelligence, machine learning, computer vision, pattern recognition, and wireless communications. In these areas, he has published five books and around 150 technical articles in refereed journals and proceedings, including the IEEE TRANSACTIONS ON IMAGE PROCESSING, the IEEE TRANSACTIONS ON CIRCUITS AND SYSTEMS FOR VIDEO TECHNOLOGY, the IEEE TRANSACTIONS ON NEURAL NETWORKS, and the IEEE TRANSACTIONS ON SYSTEMS, MAN, AND CYBERNETICS.

Dr. Gao is currently a Fellow of IET. He served as the general chair/cochair or program committee chair/cochair or PC member of around 30 major international conferences.

Bin Wang received the B.Sc. and M.Sc. degrees in electronics and information system from Northwest University, Xi’an, China, in 1999 and 2002, respectively, and the Ph.D. degree in pattern recognition and intelligent system from Xidian University, Xi’an, in 2010.

He is currently an Associate Professor with the School of Electronic Engineering, Xidian University. His current research interests include image segmentation and analysis.

Fan Yang was born in Tianjin, China, in 1963. She received the B.S. degree in electrical engineering from the University of Lanzhou, Lanzhou, China, in 1982 and the M.S. degree in computer science and the Ph.D. degree in image processing from the University of Burgundy, Dijon, France, in 1994 and 1998, respectively.

She is currently a Full Professor and a member of LE2I CNRS-UMR, Laboratory of Electronic, Computing and Image Sciences, University of Burgundy. She is a member of the French research group Information, Signal, Images and Vision, and she livens up the theme C: Algorithm Architecture Mapping. Her research interests are in the areas of pattern recognition, neural network, motion estimation based on spatial–temporal Gabor filters, parallelism and real-time implementation, and, more specifically, biometric image processing algorithms and architectures.

Vincent Brost was born in St Remy, France in 1963. He is an engineering graduate in electronics specialized in embedded system, Ecole des Mines d’Ales, France in 1990. He received the M.S. degree in electrical engineering and Ph.D. degree in image processing and electrical engineering from University of Burgundy, France, in 2000 and 2006, respectively.

He is currently an Associate Professor and a member of LE2I CNRS-UMR, Laboratory of Electronic, Computing and Image Sciences, University of Burgundy, Dijon, France. His research interests are in the areas of rapid prototyping systems, VLIW architecture, real-time image processing, and electronic devices.